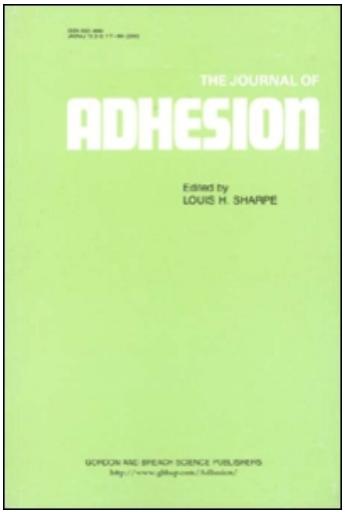

The Journal of Adhesion
Publication details, including instructions for authors and subscription information:
http://www.informaworld.com/smpp/title~content=t713453635

Adhesive Contact of a Membrane with a Hemispherical Indenter: Theoretical Analysis and Model Liquid System

Rebecca E. Webber[a]; Wendy Da Wei Cheng[a]; Kenneth R. Shull[a]
[a] Department of Materials Science and Engineering, Northwestern University, Evanston, Illinois, USA

To cite this Article Webber, Rebecca E. , Cheng, Wendy Da Wei and Shull, Kenneth R.(2006) 'Adhesive Contact of a Membrane with a Hemispherical Indenter: Theoretical Analysis and Model Liquid System', The Journal of Adhesion, 82: 5, 427 — 446
To link to this Article: DOI: 10.1080/00218460600713576
URL: http://dx.doi.org/10.1080/00218460600713576

The Journal of Adhesion, 82:427–446, 2006

ISSN: 0021-8464 print/1545-5823 online
DOI: 10.1080/00218460600713576

Taylor & Francis
Taylor & Francis Group

Adhesive Contact of a Membrane with a Hemispherical Indenter: Theoretical Analysis and Model Liquid System

Rebecca E. Webber
Wendy Da Wei Cheng
Kenneth R. Shull
Department of Materials Science and Engineering, Northwestern University, Evanston, Illinois, USA

The axisymmetric Laplace equation is solved numerically to extract contact-angle data for a flat liquid/vapor interface contacting a submerged hemispherical solid. The liquid/vapor interface is treated as a membrane, with a membrane tension equal to the surface energy of the liquid. By measuring the vertical displacement of the membrane and the projected contact area the membrane makes with the hemisphere, the contact angle and correspondingly the driving force for motion of the contact line can be measured. We show that characteristic receding and advancing contact angles can be obtained by measuring the contact radii formed upon initial contact between the interface and hemisphere and final contact just prior to detachment of the interface, respectively. Use of the technique is illustrated with a model experiment involving the contact of an air/water interface with a poly(methyl methacrylate) surface.

Keywords: Adhesion; Dynamic contact angles; Laplace equation; Wetting

1. INTRODUCTION

Adhesion of soft materials is often probed by bringing a rigid, hemispherical indenter of radius R into contact with a flat, compliant surface. The variables that are commonly measured are the normal displacement, δ, defined as zero when the apex of the hemisphere is coincident with the surface of the elastic material; the normal load,

Received 15 November 2005; in final form 20 January 2006.
One of a collection of papers honoring Hugh R. Brown, who received *The Adhesion Society Award for Excellence in Adhesion Science, Sponsored by 3M*, in February 2006.
Address correspondence to Kenneth R. Shull, Department of Materials Science, 2220 Campus Drive, Northwestern University, Evanston, IL 60208-3108, USA. E-mail: k-shull@northwestern.edu

P; and the contact radius of the circular region of contact between the two materials, a. For nonadhesive materials, the contact radius increases smoothly from zero as the compressive displacement increases. The relationship between a and δ in this nonadhesive case is purely geometrical, and for small values of a/R the following relationship is obtained [1]:

$$a = (\delta R)^{1/2}. \tag{1}$$

Adhesive interactions cause the contact radius to be larger than the value predicted by Equation (1), as quantified originally by Johnson, Kendall, and Roberts (JKR) [2]. The effect can be quantified by the following relationship of the energy release rate, $\mathcal{G}$; the displacement; and the contact radius:

$$\mathcal{G} = \frac{E^*(a^2/R - \delta)^2}{2\pi a}, \tag{2}$$

with $E^* = E/(1-\nu^2)$, where E is Young's modulus and ν is Poisson's ratio for the compliant material [3]. The contact radius for $\delta = 0$, which we define as a_{0b}, is given by the following expression:

$$\frac{a_{0b}}{R} = [2\pi]^{1/3}\left(\frac{\mathcal{G}}{E^*R}\right)^{1/3}. \tag{3}$$

Under equilibrium conditions, $\mathcal{G}$ can be viewed as the adhesion energy. The requirement that a_{0b}/R be small is equivalent to requiring a small value of $\mathcal{G}/E^*R$. In many commonly employed cases, this condition is quite easily met. For equilibrium contact of small silicone elastomers, for example, representative values are $0.05\,\mathrm{J/m^2}$ for $\mathcal{G}$, 10^6 Pa for E, and 10^{-3} m for R, giving $\mathcal{G}/ER \approx 5\times10^{-5}$ and $a_{0b}/R \approx 0.06$ (with $\nu = 0.5$). The appeal of JKR-type experiments in this regime is that Equations (2) and (3) remain valid, yet the contact radii are large enough to be measured easily. The typical JKR geometry is shown in Figure 1a.

A consequence of Equation (2) is that low-modulus materials are required to measure very low values of the adhesion energy, $\mathcal{G}$. However, the use of very soft materials poses an additional problem, even if the ratio $\mathcal{G}/ER$ remains small. In these situations, surface deformations become more important than bulk deformations and can dominate the behavior. In other words, work done against the interfacial tension, γ, becomes more important than work done against bulk elasticity of the compliant material. In the liquid limit ($E \to 0$), the contact radius is determined by a balance of adhesion energy and interfacial tension. The situation is conceptually identical to the illustration in Figure 1b, which shows a membrane that has been expanded into contact with a

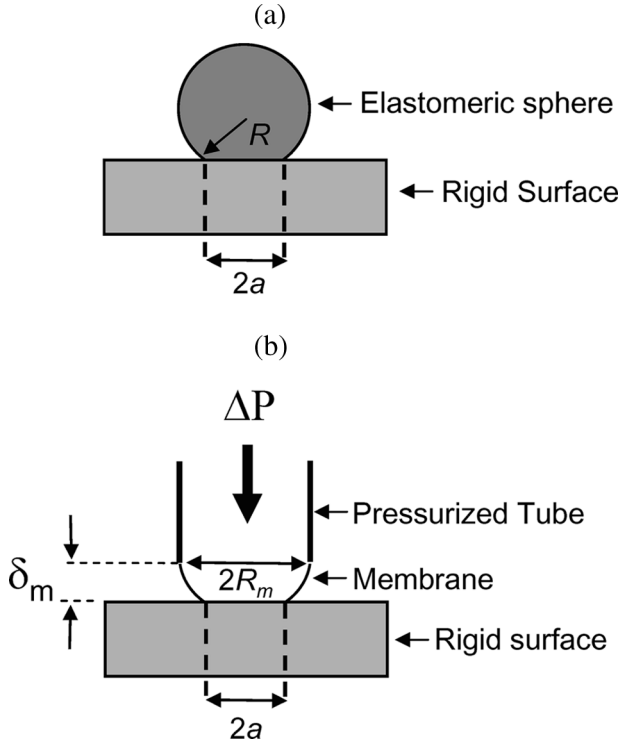

FIGURE 1 Contact of curved materials with a flat surface: (a) compliant hemisphere (JKR geometry), and (b) membrane geometry formed by applying pressure to one side of an initially flat membrane.

surface by the application of a pressure difference, ΔP. In general, the tension of this membrane is determined by the elastic deformation of the membrane and by its surface energy. Because the membrane in our case is an analog of the free surface of a material, we ignore elastic effects and assume the membrane tension is equal to γ in the rest of our discussion. Elastic contributions to the membrane have been considered by Wan and Kogut for this geometry for the case where $\Delta P = 0$ [4], and in the recent experiments of Raegen *et al.* [5]. Similar geometries have also been suggested by Shanahan, whose early contributions have influenced much of this more recent work [6,7].

In the membrane-contact problem of interest to us (Figure 1b), the membrane is originally circular with a radius of R_m and is then pressurized to form a curved surface with radius of curvature R. The pressure difference required to produce this curvature is $2\gamma/R$.

Prior to contact, the center of the membrane is displaced from the edge by a distance equal to $R_m^2/2R$, assuming that displacement is small compared with R_m. Contact of the membrane with the surface occurs when this central displacement is equal to δ_m, the distance between the supported edge of membrane and contacting surface. Therefore, the pressure difference required to initiate contact is equal to $4\gamma\delta_m/R_m^2$. If ΔP remains fixed at this value, and there is no adhesion present to increase the contact area, the membrane/substrate contact radius will be equal to zero at this point. Adhesive interactions increase the contact radius, giving a membrane with the shape illustrated in Figure 2. As described in the Appendix, the following expression is obtained for the shape of the membrane, provided that its slope is small ($|dz/dr| \ll 1$):

$$z = \frac{\delta_m}{R_m^2}\left\{\frac{a_{0s}^2 \ln(r/a_{0s})}{\ln(R_m/a_{0s})} + r^2 - a_{0s}^2\right\}. \tag{4}$$

Here a_{0s} is the specific value of the contact radius at the pressure required for the center of the membrane to make contact with the surface. The subscript s indicates that this is the value for surface deformation, as opposed to the bulk deformation. The contact angle that the membrane makes with the surface is given by the following expression:

$$\theta \approx \tan\theta = \left.\frac{dz}{dr}\right|_{r=a_{0s}} = \frac{a_{0s}\delta_m}{R_m^2}\left(2 - \frac{1}{\ln(a_{0s}/R_m)}\right). \tag{5}$$

The contact angle is significant in the context of adhesion, because it can be directly used to obtain the adhesion energy from the following

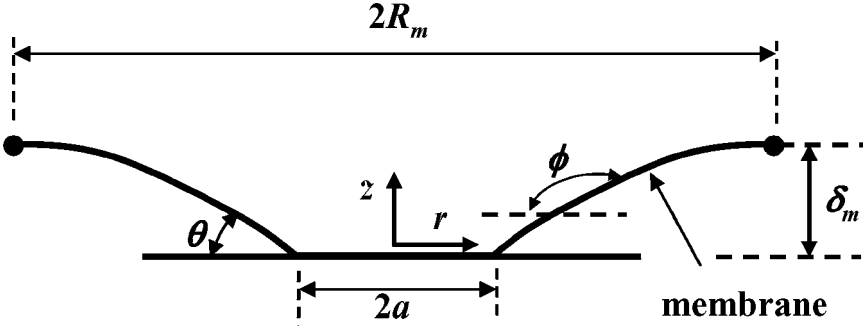

FIGURE 2 Detailed schematic illustration of the membrane shape for the geometry illustrated in Figure 1b.

general relationship:

$$\mathcal{G} = \gamma(1 - \cos\theta) \approx \frac{\gamma\theta^2}{2} \tag{6}$$

for which we have invoked the small angle approximation that is consistent with the geometric approximations already made. By combining Equations (5) and (6), we obtain the following expression for the energy-release rate for the membrane case:

$$\mathcal{G} = 2\gamma \frac{a_{0s}^2 \delta_m^2}{R_m^4} \left(1 - \frac{1}{2\ln(a_{0s}/R_m)}\right)^2. \tag{7}$$

For small values of a_{0s}/R_m, the following expression is obtained from rearrangement of Equation (7):

$$\frac{a_{0s}}{R_m} \approx \left(\frac{2\mathcal{G}}{\gamma}\right)^{1/2} \approx \theta. \tag{8}$$

The assumption of the JKR analysis [Equations (2) and (3)] is that $a_{0s} \gg a_{0b}$, so that the contact radius is not limited by surface deformations. As the sample size decreases and the surface-to-volume ratio increases, surface deformations become increasingly important and eventually dominate the response. We define R_{crit} as the critical value of R below which surface deformations dominate the response. We can obtain this parameter from Equations (3) and (8) with the condition that $a_{0s} = a_{0b}$ for $R = R_{crit}$:

$$R_{crit} = \pi \frac{\gamma}{E^*} \left(\frac{\gamma}{2\mathcal{G}}\right)^{1/2} = \frac{\pi}{\theta} \frac{\gamma}{E^*}. \tag{9}$$

Some insight into the relevance of Equations (8) and (9) is obtained by considering the behavior of gels with $\gamma \approx 0.03\,\mathrm{J/m^2}$ and $E^* \approx 10^4\,\mathrm{Pa}$. For these gels, R_{crit} exceeds 1 mm for values of $\mathcal{G}$ that are less than $1.3 \times 10^{-6}\,\mathrm{J/m^2}$, corresponding to contact angles less than 0.01 rad. (0.5°). This value for $\mathcal{G}$ represents a very small adhesion energy and enables surface deformations to be ignored in bulk contact mechanics experiments in most practical situations. However, there are two important exceptions. The first of these are experiments with very soft gels, or with submicron latex particles, where γ/E^*R is large enough so that surface deformations need to be taken into account [8,9]. The second important exception involves experiments that are designed to take advantage of the membrane geometry itself. A functional membrane designed to have specific interactions can be prepared, for example, by spreading appropriately chosen surfactant molecules at an air/water

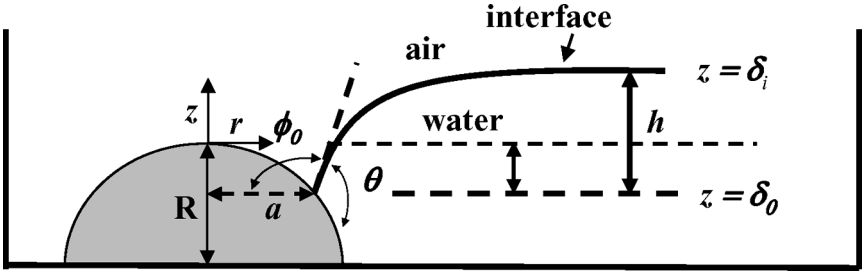

FIGURE 3 Schematic of the interfacial test geometry and relevant parameters for analysis.

water interface. The significance of this analysis is that the contact angle, and hence the adhesion energy, can be obtained from measurements of the contact radius, provided that δ_m and R_m are known.

In this article we describe some simple model experiments in which the contact angle is obtained from a measure of the contact radius. We make use of the simplest possible model system, where the membrane is an air/water interface. Also, instead of applying a pressure to generate a curved interface that interacts with a flat, rigid surface, we invert the curvature and study the interaction of a curved, rigid hemisphere with an initially flat interface, as illustrated in Figure 3. This inverted geometry is experimentally easier to implement and has been used for this reason. Because two conditions required to obtain analytical solutions are not valid for this problem, a numerical analysis is applied to obtain an expression for the contact angle. First, the density difference of the media on either side of the interface is no longer zero, so that variations in the hydrostatic pressure need to be taken into account. Second, the slope of the interface is not necessarily small. For both reasons a full solution of the axisymmetric Laplace equation for the shape of the interface must be employed. Our method of solution is formulated here, followed by a description of the application of these results to measurements of contact angles.

2. THEORETICAL APPROACH

Our experimental geometry, illustrated schematically in Figure 3, involves the placement of a glass hemisphere at the bottom of a glass dish. The dish is subsequently filled with water to cover the hemisphere, and a syringe pump is used to raise and lower the water level. During the course of an experiment, the measured quantities are δ_i, the displacement of the water level relative to the apex of the

hemisphere, and a, the projected radius of the dry patch at the center of the hemisphere. A polar coordinate system originates at the apex of the hemisphere, with r representing the radial distance away from the axis of symmetry, and z representing the distance along the axis of symmetry. Because the interface flattens as a result of gravity, ϕ (defined in Figure 2) approaches 180° for large values of r, where the displacement of the interface with respect to the apex of the sphere is equal to δ_i. Other relevant parameters are δ_0, the z coordinate of the surface of the hemisphere at $r = a$, and h, the total vertical displacement of the interface, which are related to one another as follows:

$$\delta_0 = \delta_i - h = \sqrt{R^2 - a^2} - R. \tag{10}$$

At the three-phase contact line, where the air/water interface meets the hemisphere, ϕ is equal to ϕ_0, which is related to the contact angle by the following geometric relationship:

$$\phi_0 = 180^\circ - \theta + \arctan\left(\frac{1}{\sqrt{(R/a)^2 - 1}}\right). \tag{11}$$

Equation (11) enables the contact angle to be determined from ϕ_0, which is in turn obtained from the solution to the axisymmetric Laplace equation as described next.

2.1. Axisymmetric Laplace Equation

The boundary conditions for the shape of the interface in this problem are $\phi = \phi_0$ and $z = \delta_0$ at $r = a$, and $\phi = 180^\circ$ and $z = \delta_i$ for $r \to \infty$. Our solution is an adaptation of the solutions presented by Rooks *et al.* [10], and also by Timoshenko and Woinowsky-Krieger [11]. Our starting point is the Laplace equation obtained by equating the hydrostatic pressure with the pressure associated with the interface curvature:

$$\Delta\rho g(\delta_i - z) = \gamma\left(\frac{1}{R_1(z)} + \frac{1}{R_2(z)}\right), \tag{12}$$

where $\Delta\rho$ is the difference in density between the oil and water phases, g is the gravitational acceleration, and $R_1(Z)$, $R_2(Z)$ are the principal radii of curvature of the interface, given by the following expressions:

$$R_1(z) = -\frac{1}{\sin\phi}\frac{dz}{d\phi}, \tag{13}$$

$$R_2(z) = \frac{r}{\sin\phi}. \tag{14}$$

The pressure is equal to zero at $z = \delta_i$, where the interface is flat, and increases to $\Delta\rho g h$ at $z = \delta_0$. Equation (12) can be written in non-dimensional form by using the capillary length, C, to obtain the two dimensionless distances X and Y [10]:

$$C = \left(\frac{\gamma}{\Delta\rho g}\right)^{1/2}, \quad X \equiv \frac{r}{C}, \quad Y \equiv \frac{z}{C}. \tag{15}$$

After some rearrangement, the following form of the Laplace equation results from the combination of Equations (12)–(15):

$$\frac{dY}{d\phi} = \frac{X \sin\phi}{XY + \sin\phi - (Xh/C)}. \tag{16}$$

A related expression for $dX/d\phi$ is obtained from the fact that $dz/dx = -\tan\phi$:

$$\frac{dX}{d\phi} = \frac{-X \cos\phi}{XY + \sin\phi - (Xh/C)}. \tag{17}$$

Equations (16) and (17) describe the evolution of r and z with ϕ. The balance of the Laplace pressure and gravitational forces determines the shape of the interface, as ϕ asymptotically approaches 180° because of gravitational flattening. To solve these equations, we employ a shooting method where ϕ_0 is adjusted iteratively until the value obtained for h agrees with the desired (or experimental) value.

2.2. Numerical Solutions

The qualitative behavior of the system is determined by the relative values of the two characteristic lengths in the problem, the radius of curvature of the hemisphere, R, and the capillary length, C. Characteristic behavior for different values of C/R is illustrated in Figure 4, where we show calculated interface profiles for $C/R = 10^4$ (part a), $C/R = 0.9$ (part b), and $C/R = 0.1$ (part c). For each of these calculated profiles, $a/R = 0.3$, $\theta = 70°$, and, from Equation (11), $\phi_0 = 132.5°$. The capillary length for pure water ($\rho = 1\,\mathrm{g/cm^3}$ and $\gamma = 72\,\mathrm{erg/cm^2}$) is 2.7 mm, making the data for C/R correspond to our experimental system, in which we use a glass hemisphere with $R = 3\,\mathrm{mm}$. The capillary length is the characteristic distance over which gravitational flattening affects the shape of the interface. For very large values of C/R, as in Figure 4a, the shape of the interface in the vicinity of the hemisphere is not perturbed by gravity. If the interface slope is small (ϕ_0 close to 180°), the shape of the interface is given by the following adaptation of Equation (4):

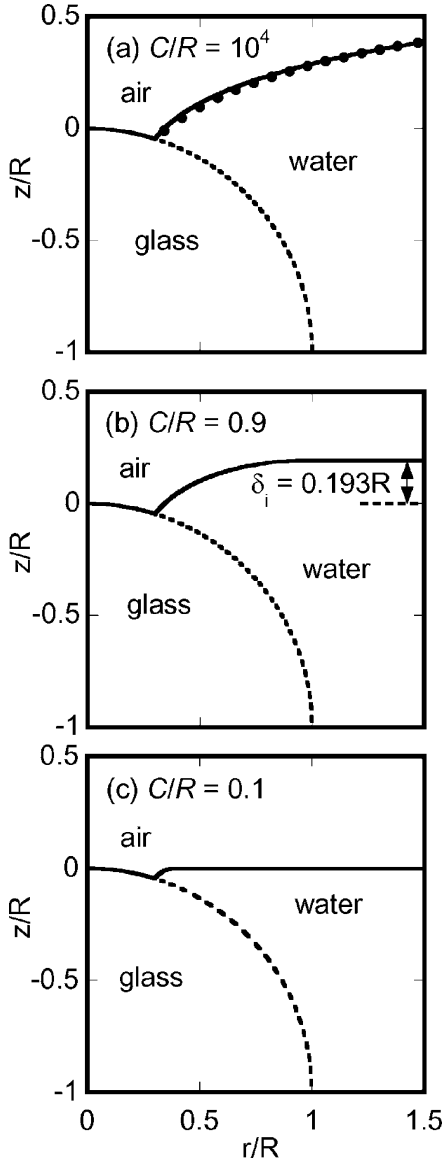

FIGURE 4 Example interfacial profiles for $a/R = 0.3$ and $\theta = 70^\circ$. The different plots correspond to different values of the normalized capillary length, C/R, using the values indicated on each plot. The dotted line in each case is the outline of the hemisphere, and the solid line is the solution to the full Laplace equation obtained as outlined in Section 2. The symbols in the top figure represent Equation (18), with $a = 0.3R$ and $R_m = 1.5a$.

$$z = \delta_0 + \frac{a^2 h'}{R_m^2}\left\{\frac{\ln(r/a)}{\ln(R_m/a)} + r^2 - a^2\right\}. \quad (18)$$

Here h' is the vertical distance between the interface position at $r = R_m$ and $r = a$. The circles plotted along the interface in Figure 4a represent the fit to Equation (18), where we have taken $R_m = 1.5a$.

Equation (18) is valid for small interface slopes and for values of r that are much less than the capillary length. In this regime no single, well-defined value for h' exists, because it depends on the value that is chosen for R_m. Experimentally, this regime is not as useful as the regime for large values of r, where gravitational flattening gives an asymptotic value for h' (which we refer to simply as h) and a well-defined value for the closely related interface displacement, δ_i. The calculated interface profiles shown in Figures 4b and 4c show the existence of a well-defined, asymptotic interface height. Because Equation (18) is no longer valid for these large values of R_m, the full numerical solutions need to be employed to determine contact angles from the measured values of a and δ_i.

The control variable in an experimental determination of the contact angle is the interface displacement, δ_i, which is adjusted by adding or removing liquid from the system. The contact radius in this case is actually the projected radius of the dry patch at the top of the hemisphere, but we continue to use the contact terminology to make the connection to membrane-contact experiments. In Figure 4b, a contact radius of $0.3R$ corresponds to a contact angle of 70°. This combination of a and θ is just one combination of these parameters that satisfies the Laplace equation for $C/R = 0.9$ and $\delta/R = 0.193$. The other solutions for these values of C/R and δ/R can be illustrated by plotting θ as a function of the corresponding contact radius. In Figure 5, we show a series of these types of curves, for each of the three values of C/R used to generate the data in Figure 4. Each of the three plots includes a series of curves for the same value of C/R but with different values of δ_i/R.

Use of the curves shown in Figure 5 can be illustrated by considering the case for $C/R = 0.9$, which corresponds to our experimental situation of an air/water interface in contact with a hemisphere with $R = 3$ mm. An experiment is generally conducted by completely immersing the hemisphere in water and then carefully withdrawing water until $\delta_i = 0$, where the air/water interface hits the apex of the hemisphere. At this point, the contact area grows rapidly, and the contact angle evolves along the dashed line in Figure 5b. The contact angles along this $\delta_i = 0$ line, corresponding to the original contact of the interface, are referred to as θ_0. Note that θ_0 is a receding contact

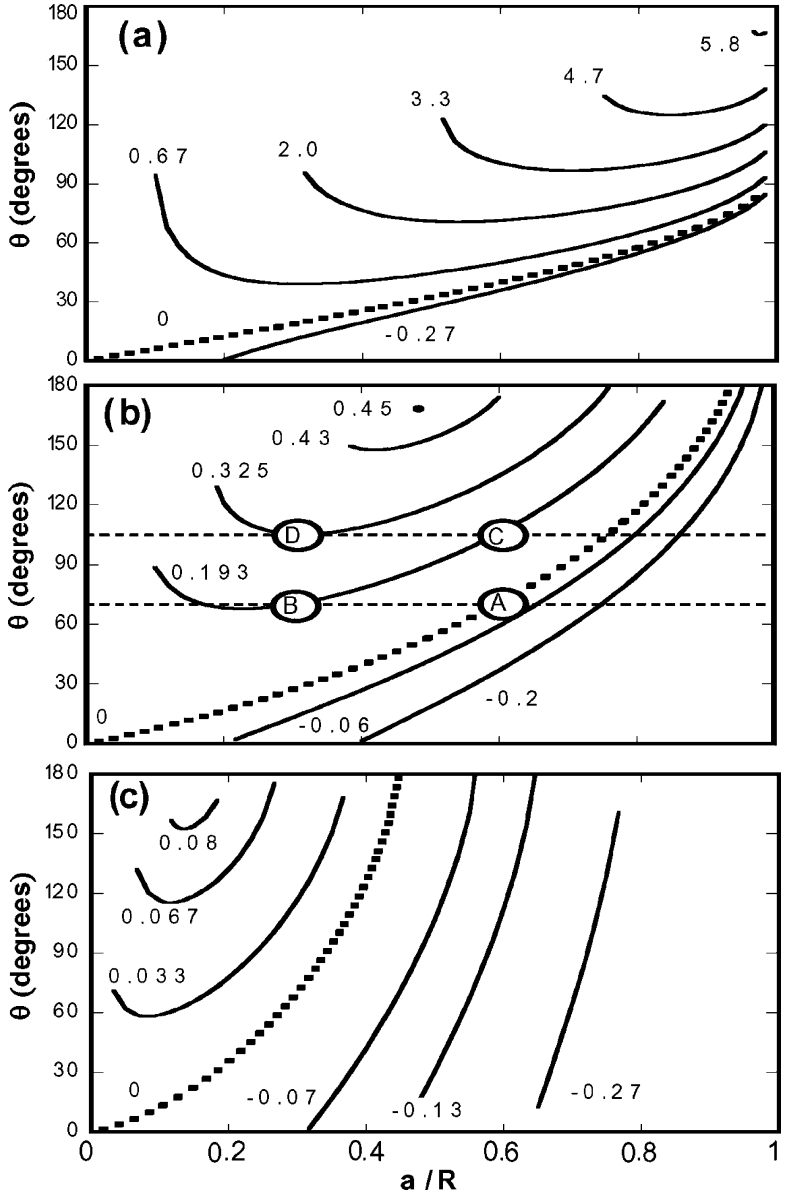

FIGURE 5 Calculated contact curves as a function of a/R, for different combinations of δ_i/R and C/R. Each of the three plots has a series of curves for a fixed value of C/R (10^4 for (a), 0.9 for (b), and 0.1 for (c)). The numbers by each curve represent the value of δ_i/R corresponding to that curve. The labeled symbols in (b) are explained in the text.

angle because the contact line is moving toward the liquid phase as a increases during this portion of the experiment. If δ_i remains fixed at zero, the contact radius will stop growing at the point where θ_0 is equal to the static receding contact angle. Point A in Figure 5b corresponds to the situation where this contact angle is 70°. The rapid growth of the contact radius when the interface makes contact with the hemisphere gives a clear signature of the point where $\delta_i = 0$.

Once the interface makes initial contact with the hemisphere, additional liquid can be added or withdrawn, resulting in further changes in δ_i. Changes in the interface displacement shift the curves relating the contact angle and the contact radius, with positive changes in the displacement moving the curves to higher contact angles and lower contact radii. If the contact angle remains fixed, increasing the interface displacement will lead to a decrease in the contact radius. For example, for a contact angle of 70°, the contact radius shifts from $0.59R$ to $0.3R$ as δ_i is increased from 0 to $0.193R$. This transition corresponds to motion from point A to point B in Figure 5b.

The power of this technique for measuring contact angles is that θ can be measured as a function of the velocity of the contact line, for both advancing and receding contact. The assumptions of this approach are that the Laplace pressure throughout the liquid is equilibrated and that axial symmetry is maintained. The method requires that the - interface displacement be measured accurately. Although this can be accomplished by a variety of methods, including accurate measurement of the volume of liquid added to the system, it is useful to develop methods that can be used to obtain the estimates for the static advancing and receding contact angles without requiring an independent measure of the interface displacement. The receding contact angle can be measured from θ_0 as described previously because the jump into contact provides a discernable signature of the point where the interface displacement is equal to zero. Advancing contact angles can likewise be determined by measuring the detachment radius, a_d.

The concept of the detachment radius originates from the fact that plots of θ *vs.* a (Figure 5) have a minimum for positive values of the interface displacement. This minimum occurs at $\theta = \theta_d$ and $a = a_d$, where θ_d is the detachment contact angle and a_d is the detachment contact radius. Plots of θ_d as a function of a_d can be determined from a series of numerical calculations, each using a different value for the interface displacement. Results for $C/R = 0.1$, 0.9, and 10^4 are shown in Figure 6. The significance of θ_d and a_d can be understood by considering the behavior of an idealized system characterized by advancing and receding angles that are not dependent on the velocity of the

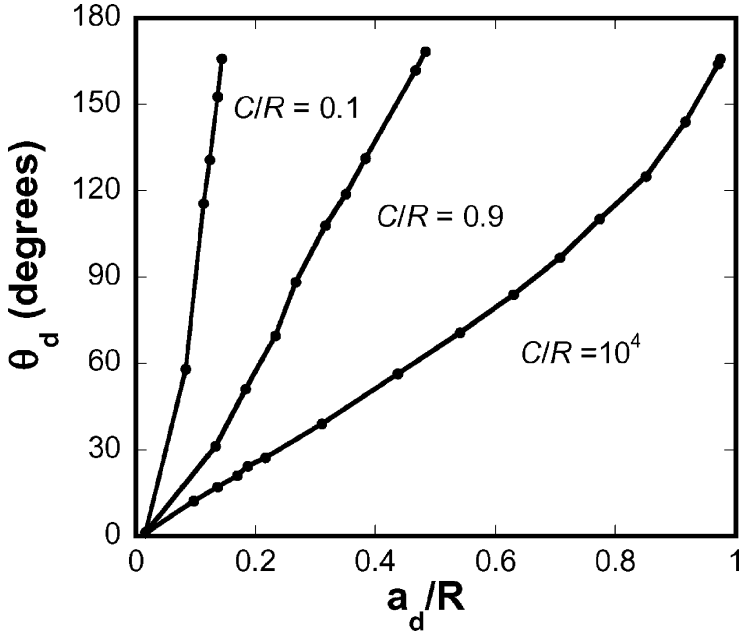

FIGURE 6 Relationship between the detachment contact angle and normalized detachment contact radius, obtained from minima of the curves plotted in Figure 5.

contact line. The specific case for a receding contact angle of 70° and an advancing contact angle of 105° is illustrated in Figure 5b. The contact radius established during initial contact is given by point A, where the horizontal line representing $\theta = 70^\circ$ intersects the contact curve for $\delta_i = 0$. When the interface displacement is increased, the contact radius remains fixed until the contact angle reaches the advancing value of 105° (point C on Figure 5b). Point C lies on the contact curve for $\delta_i = 0.193R$, so this is the interface displacement that must be applied for the contact radius to begin to shrink. Further increases in the interface displacement give decreasing values of the contact radius. If the contact angle remains fixed at 105°, the contact radius eventually shrinks to the value corresponding to point D on Figure 5b, which is the minimum of a contact curve with $\delta_i = 0.325R$. For larger values of δ_i, the contact angle exceeds 105° for all values of the contact radius. Because the contact angle exceeds 105° for the remainder of the experiment (assuming that δ_i is continuing to increase) the contact radius rapidly reduces to zero; *i.e.*, the interface detaches from the hemisphere. As a result, the detachment angle, and hence the

advancing contact angle, can be determined by measuring the contact radius where membrane detachment occurs, using the data shown in Figure 6 to convert a_d to θ_d.

The detachment process is analogous to adhesive pulloff, which is observed in elastic systems when the energy-release rate exceeds a critical value. Using the language of fracture mechanics, the contact radius will shrink whenever the energy-release rate, $\mathcal{G}$, given here by $\gamma(1 - \cos\theta)$, exceeds a critical value. In our case, the applied energy-release rate driving detachment of the interface is controlled by controlling δ_i, which in turn determines θ and hence $\mathcal{G}$.

3. MODEL EXPERIMENT

A simple set of experiments was performed to illustrate the use of the interfacial contact concepts outlined in Section 2. In these experiments, a glass hemisphere with a radius of 3 mm was used, onto which a hydrophobic surface coating was placed by spin coating a solution of poly(methyl methacrylate) in toluene. This coated hemisphere was placed in a cylindrical dish with a radius of 5 cm and was completely covered with water. A New Era Pump Systems (Farmingdale, NY, USA) syringe pump was used to add and withdraw water from the dish, with a typical pumping rate of 0.833 mL/min. This volume rate corresponds to an interfacial displacement rate of 0.42 mm/min. Images of the contact between the hemisphere and the interface were captured by a video camera attached to a Zeiss Axiovert inverted microscope with 1.25× objective lens (Ziess, Oberkochan, Germany). The projected contact radii between the interface and hemisphere were measured from digitally collected images.

Figure 7 displays a typical initial contact picture accompanied by the interfacial profile at that point for an air/water interface contacting a glass hemisphere coated with a thin layer of poly(methyl methacrylate) (PMMA). The contact area is readily discernable, and the value of θ_0 obtained from the measured contact radius is 70° (point A on Figure 5b). The advancing contact angle was obtained by increasing the interface displacement and measuring the critical contact radius just prior to the point where water completely floods the surface of the glass hemisphere. Images were taken once every second, and measured contact radii for the last 5 s of several different experiments are plotted in Figure 8. The contact line in these experiments is moving with velocities as large as 100 μm/s. As a result, the limited time resolution imposed by the video capture rates we have used gives considerable uncertainty in the actual value of a_d. This uncertainty explains a large fraction of the spread in advancing contact angles

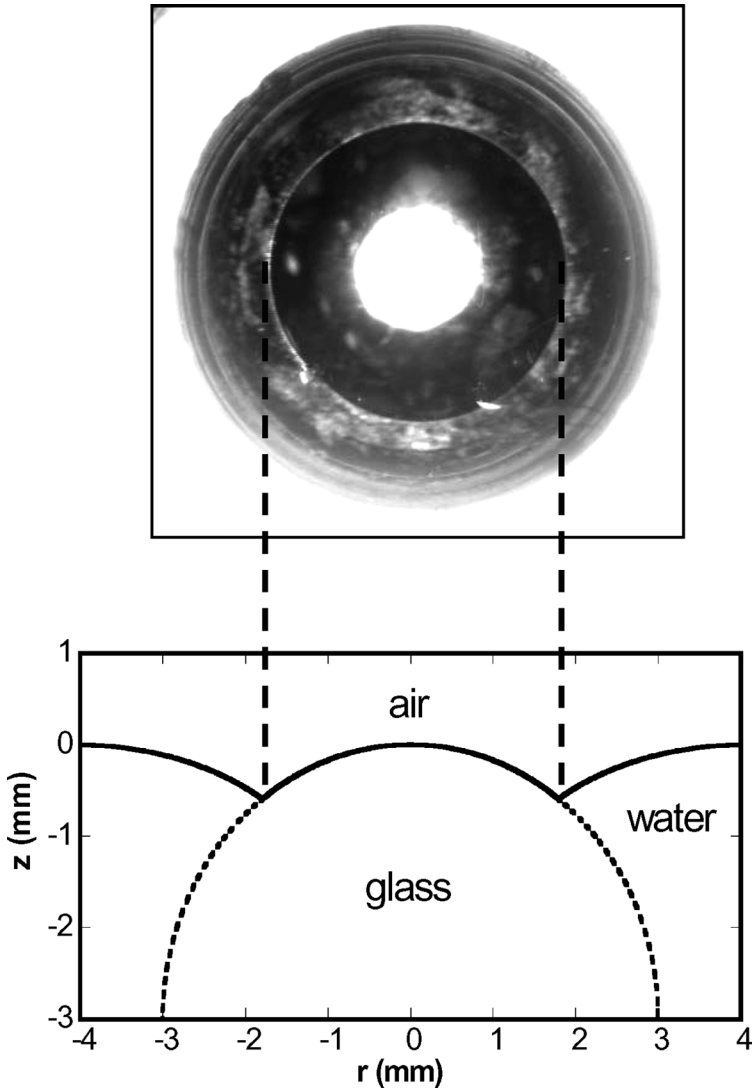

FIGURE 7 Typical contact image and interfacial profile for initial contact of an air/water interface on a PMMA-coated hemisphere (top) and the corresponding calculated interfacial profile (bottom). In this example, $R = 3\,\text{mm}$, $C = 2.7\,\text{mm}$, $a_c = 1.8\,\text{mm}$, and $\theta_0 = 70^\circ$.

determined from the relationship between a_d and θ_d that is reproduced in Figure 9. In this figure, we take the last measured value of a for each of the curves in Figure 8 (plotted as solid vertical lines in

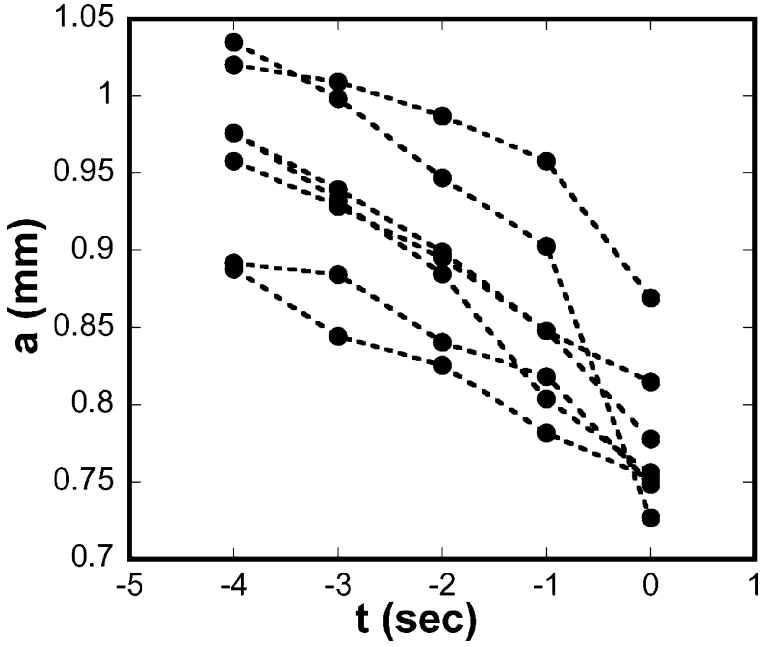

FIGURE 8 Measured contact radii from the final five images from advancing contact measurements for a PMMA-coated hemisphere with $R = 3\,\text{mm}$.

Figure 9) and convert these to contact angles using the relationship between a_d and θ_d that is valid for $R = 3\,\text{mm}$ and $C = 2.7\,\text{mm}$. Values of θ_d corresponding to these contact radii vary from 77° to 98°. This analysis assumes that the system evolves such that adhesive detachment of the interface occurs at the point of the instability, but the actual behavior involves a more complicated interplay of the relationship between the dynamic contact angle and velocity at which the contact radius is decreasing [12]. A more complete approach involves the accurate determination of the interface displacement, so that the contact angle can be determined directly from the values of δ_i and a.

4. SUMMARY AND CONCLUSIONS

In this article we have described a membrane-contact geometry that can be used to measure adhesive interactions. Analytic expressions are available for small deformations in situations where the pressure difference across the membrane can be ignored. The simple model system to which we have applied this analysis is an air/water interface.

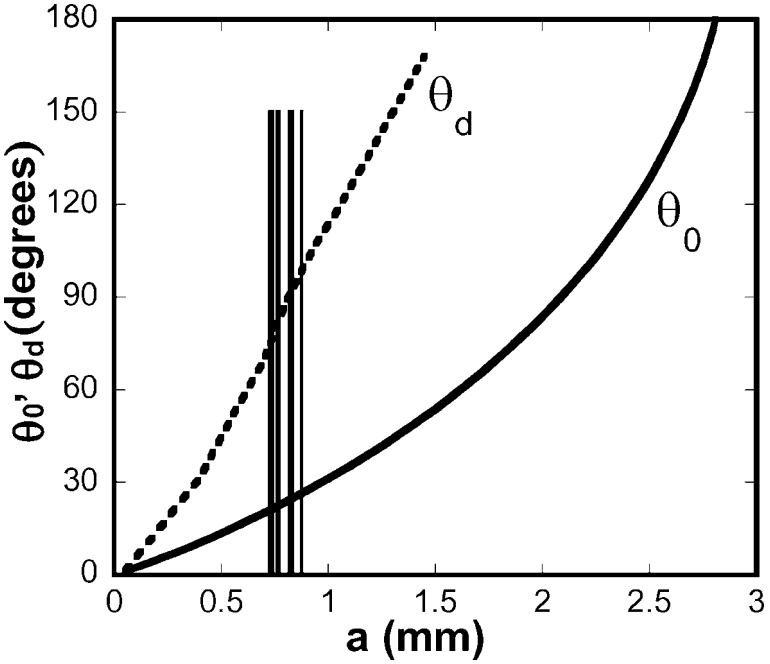

FIGURE 9 Calculated values of θ_0 and θ_d for $C = 2.7\,\text{mm}$ and $R = 3.0\,\text{mm}$. The vertical lines correspond to the final contact radii from the curves shown in Figure 8 and are used to obtain measured values of θ_d.

In this case the analytic solutions cannot be applied, and the contact angle is obtained from measured values of the displacement and contact radius using the numerical solution to the axisymmetric Laplace equation. Two contact angle values can be measured without the need to directly measure the displacement of the interface relative to the glass surface used in these experiments. The first of these is the receding contact angle made when the interface first comes into contact with surface. The second of these is the advancing angle, corresponding to the detachment instability that occurs when the dry patch at the surface suddenly vanishes as the interface displacement is increased.

As applied to the experiments performed with the PMMA-coated glass hemispheres, the contact angles that we determine with this method are in agreement with those we obtain from the same systems from more conventional methods, which involve direct visualization of advancing and receding droplets. However, the advantage of the membrane geometry proposed here is that the flat air/water interface can be easily modified in a variety of ways. For example, functional

Langmuir monolayers can be spread at the air/water interface [13], and the interactions of these monolayers with various submerged surfaces can be studied. The technique is very well suited for exploring biological interactions across aqueous media, and these are the types of problem to which the method is currently being applied.

ACKNOWLEDGMENT

This work was supported by the National Institutes of Health (R01 DE14193) and by a grant from the Human Frontier Science Program.

APPENDIX: MECHANICS OF MEMBRANE CONTACT FOR SMALL DEFORMATIONS

For the special case of a zero density difference across the interface, Equations (12)–(14) reduce to the following:

$$\gamma\left(-\sin\phi\frac{d\phi}{dz}+\frac{\sin\phi}{r}\right)=\Delta P, \tag{19}$$

with $\tan\phi=-dz/dr$. If the magnitude of dz/dr is small (ϕ close to 0 or 180°) this equation simplifies further:

$$\frac{d^2z}{dr^2}+\frac{1}{r}\frac{dz}{dr}=\frac{\Delta P}{\gamma}. \tag{20}$$

From the boundary conditions illustrated in Figure 2 ($z=0$ at $r=a$ and $z=\delta_m$ at $r=R_m$), we obtain the following solution for the shape of the membrane:

$$z=\frac{\ln(r/a)}{\ln(R_m/a)}\left\{\delta_m-\frac{\Delta P(R_m^2-a^2)}{4\gamma}\right\}+\frac{\Delta P(r^2-a^2)}{4\gamma}. \tag{21}$$

It is useful here to introduce the inflation pressure, P_0, which is required to produce the displacement of δ_m and bring the initially flat membrane into contact with the surface:

$$\Delta P_0=\frac{4\gamma\delta_m}{R_m^2}. \tag{22}$$

Equation 4 is obtained by taking $\Delta P=\Delta P_0=4\gamma\delta_m/R_m^2$. An expression for general values of the applied pressure is obtained by writing

$\Delta P = \Delta P_0 + P_{xs}$. Equation (21) can then be written in the following form:

$$\frac{z}{\delta_m} = -\frac{\ln(r/a)}{\ln\zeta}\left\{\zeta^2 + \frac{P_{xs}}{\Delta P_0}(\zeta^2 - 1)\right\} + \left(1 + \frac{P_{xs}}{P_0}\right)\left\{\left(\frac{r}{R_m}\right)^2 - \zeta^2\right\} \quad (23)$$

with $\zeta \equiv a/R_m$. The contact angle against a flat surface is given by the following expression:

$$\theta = \left.\frac{dz}{dr}\right|_{r=a} = -\frac{\delta_m}{R_m \zeta \ln\zeta}\left\{\zeta^2 + \frac{P_{xs}}{\Delta P_0}(\zeta^2 - 1)\right\} + \frac{2\zeta\delta_m}{R_m}\left(1 + \frac{P_{xs}}{\Delta P_0}\right). \quad (24)$$

The expression for the contact angle is simplified considerably for two special cases. The first of these corresponds to the case where the pressure is fixed at the inflation pressure, *i.e.*, $P_{xs} = 0$, in which case the following expression is obtained for the contact angle:

$$\theta = \frac{\zeta\delta_m}{R_m}\left(1 - \frac{1}{2\ln\zeta}\right). \quad (25)$$

If the pressure difference is relaxed to zero after the contact is made ($P_{xs} = -\Delta P_0$), we obtain.

$$\theta = \frac{-\delta_m}{R_m \zeta \ln\zeta}. \quad (26)$$

In each case, expressions for the energy release rate are obtained from the small angle approximation of Equation (6), *i.e.*, $\mathcal{G} = \theta^2/2$. The $\mathcal{G}$ expression for $\Delta P = 0$ is equivalent to the expression that has been given previously by Wan and Kogut, who also provide a generalized version that accounts for elastic contributions to the membrane tension [4].

REFERENCES

[1] Hertz, H. and Reine, J., *Angew. Math.* **92**, 156–171 (1882).
[2] Johnson, K. L., Kendall, K., and Roberts, A. D., *Proc. R. Soc. Lond. A.* **324**, 301–313 (1971).
[3] Maugis, D. and Barquins, M., *J. Phys. D: Appl. Phys.* **11**, 1989–2023 (1978).
[4] Wan, K.-T. and Kogut, L., *J. Micromechanics Microengineering* **15**(4), 778–784 (2005).
[5] Raegen, A. N., Dalnoki-Veress, K., Wan, K.-T., and Jones, R. A. L., *Eur. Phys. J. E.* (submitted).
[6] Shanahan, M. E. R., *J. Adhes.* **63**(1–3), 15–29 (1997).

[7] Shanahan, M. E. R., *C.R. Acad. Sci. Paris, Ser. IV* **1**, 517–522 (2000).
[8] Portigliatti, M., Koutsos, V., Hervet, H., and Leger, L., *Langmuir* **16**(16), 6374–6376 (2000).
[9] Joanny, J. F., Johner, A., and Vilgis, T. A., *European Physical Journal E: Soft Matter* **6**(3), 201–209 (2001).
[10] Rooks, S., Racz, L. M., Szekely, J., Benhabib, B., and Neumann, A. W., *Langmuir* **7**(12), 3222–3228 (1991).
[11] Timoshenko, S. and Woinowsky-Krieger, S., *Theory of Plates and Shells* (McGraw-Hill, New York, 1959).
[12] Kwok, D. Y., Leung, A., Lam, C. N. C., Li, A., Wu, R., and Neumann, A. W., *J. Colloid Interface Sci.* **206**(1), 44–51 (1998).
[13] Blankenburg, R., Meller, P., Ringsdorf, H., and Salesse, C., *Biochemistry* **28**(20), 8214–8221 (1989).